Supplementary Material: Little evidence of reduced global tropical cyclone activity following volcanic eruptions

Suzana J. Camargo[1] and Lorenzo M. Polvani[2]
1 Lamont-Doherty Earth Observatory, Columbia University, Palisades, NY
2 Department of Earth and Environmental Sciences and Department of Applied Physics and Applied Mathematics, Columbia University, New York, NY

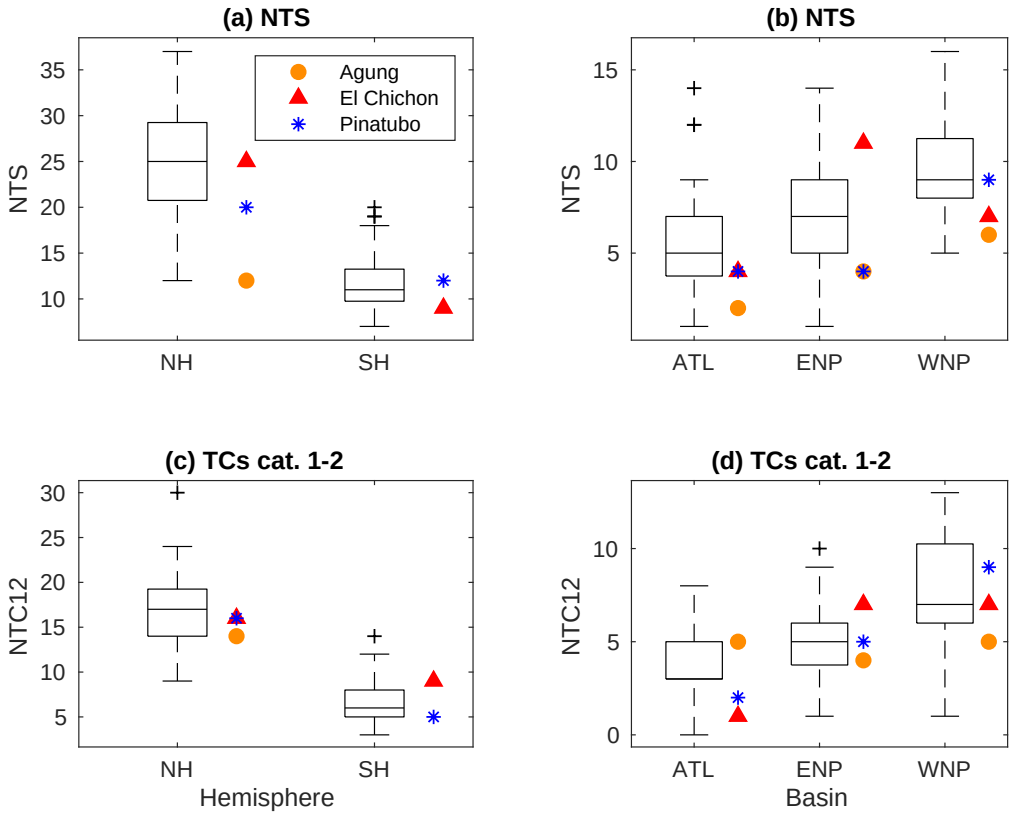

Supplementary Figure 1: The box plots (25th to 75th percentiles, central marks indicate the median) show the climatological distribution of the number of tropical storms (NTS) ((a) and (b)), and tropical cyclones with categories 1-2 NTC12 ((c) and (d)). NTC and NTC12 are counts. The whiskers show the range of the most extreme points not considered outliers, which are marked using +. Colored symbols show the values of these quantities for the first TC season after the volcanoes eruptions. Values for the NH (1961-2017) and SH (1979-2017) are shown in the left panels, three NH basins (1961-2017): Atlantic (ATL), eastern North Pacific (ENP) and western North Pacific (WNP) in the right panels.

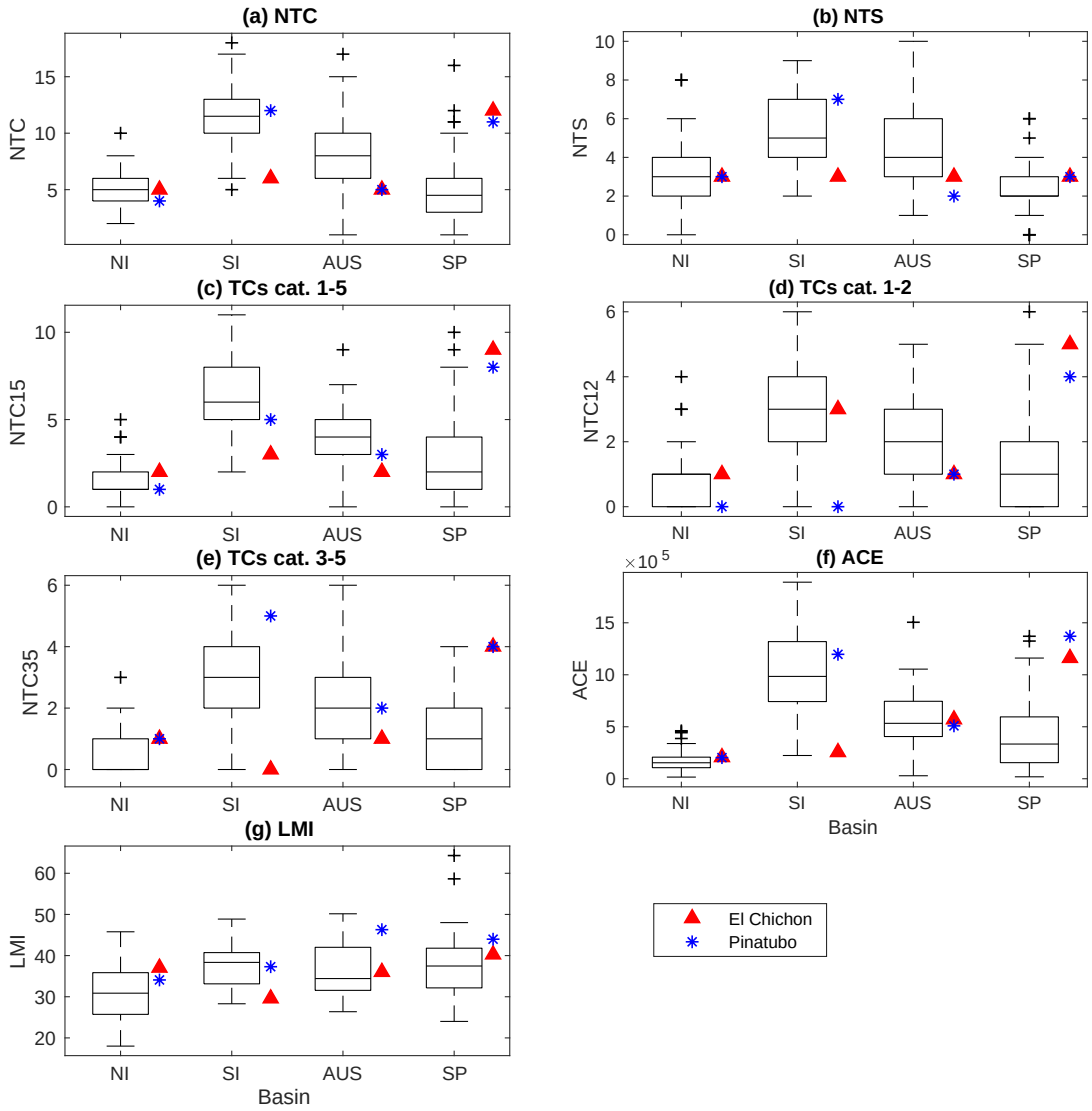

Supplementary Figure 2: Distributions and values for the first TC season after volcanoes eruptions (as described in Fig. S1) for the variables (a) NTC, (b) NTS, (c) NTC15, (d) NTC12, (e) NTC13, (f) ACE, and (g) LMI (as defined in Methods) for the North Indian Ocean (NI), South Indian Ocean (SI), Australian basin (AUS) and South Pacific for the period 1979-2017. ACE is in $(m/s)^2$ and LMI is in m/s, the other variables are counts.

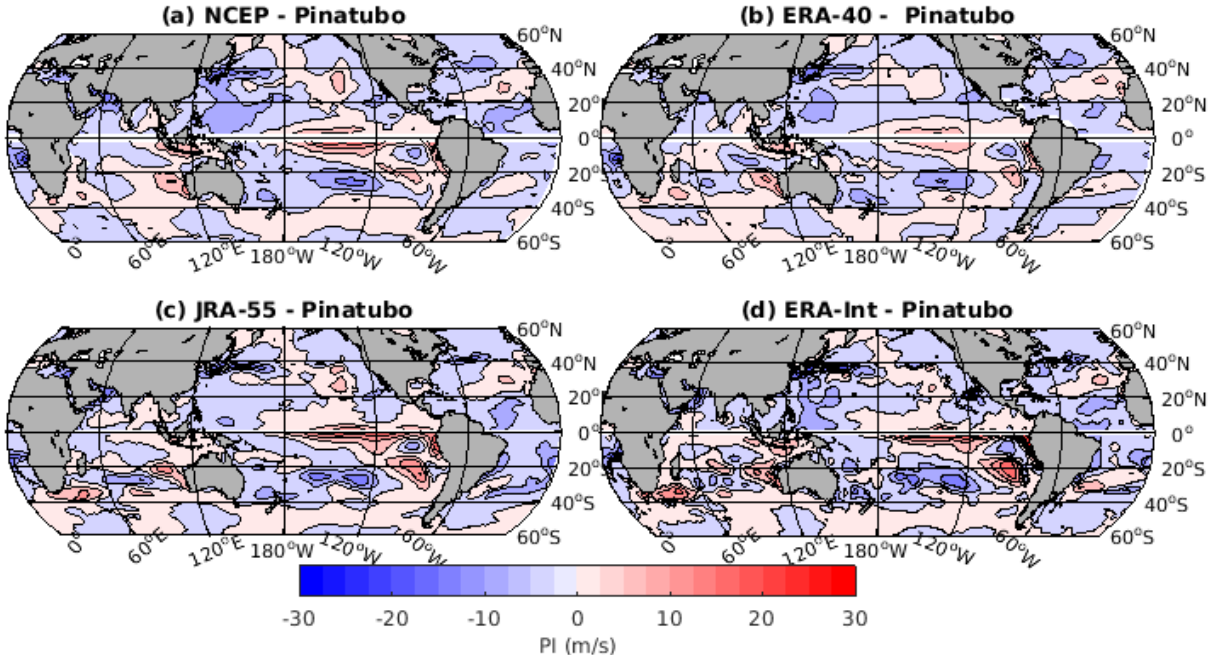

Supplementary Figure 3: Potential intensity anomalies in four reanalysis datasets in the first TC season following the eruption of Pinatubo: August to October of 1991 in the northern hemisphere, January to March of 1992 in the southern hemisphere.

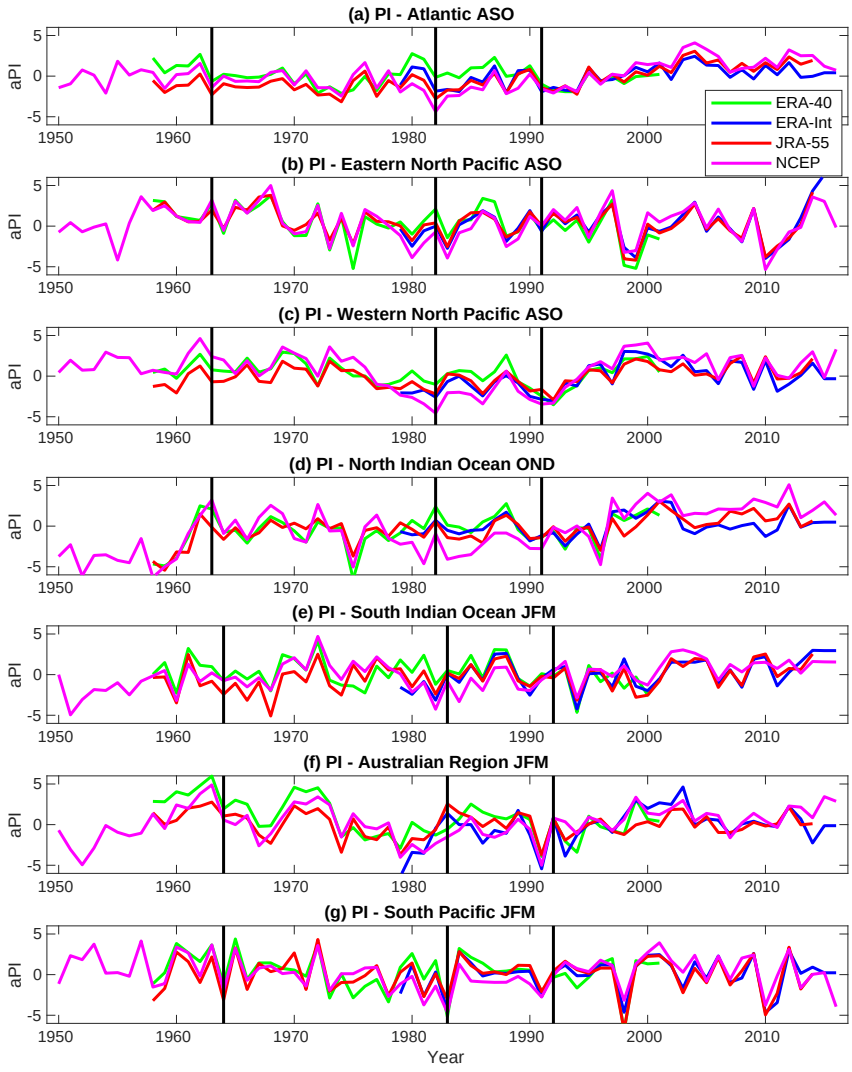

Supplementary Figure 4: Time-series of the potential intensity (PI) anomalies in reanalysis: ERA-40 (green), ERA-Interim (blue), JRA-55 (red) and NCEP (pink) for all basins in their peak season (August to October (ASO); October to December (OND) or January to March (JFM)). PI is given in m/s. The first TC season in each hemisphere after large volcanic eruptions are marked in black.

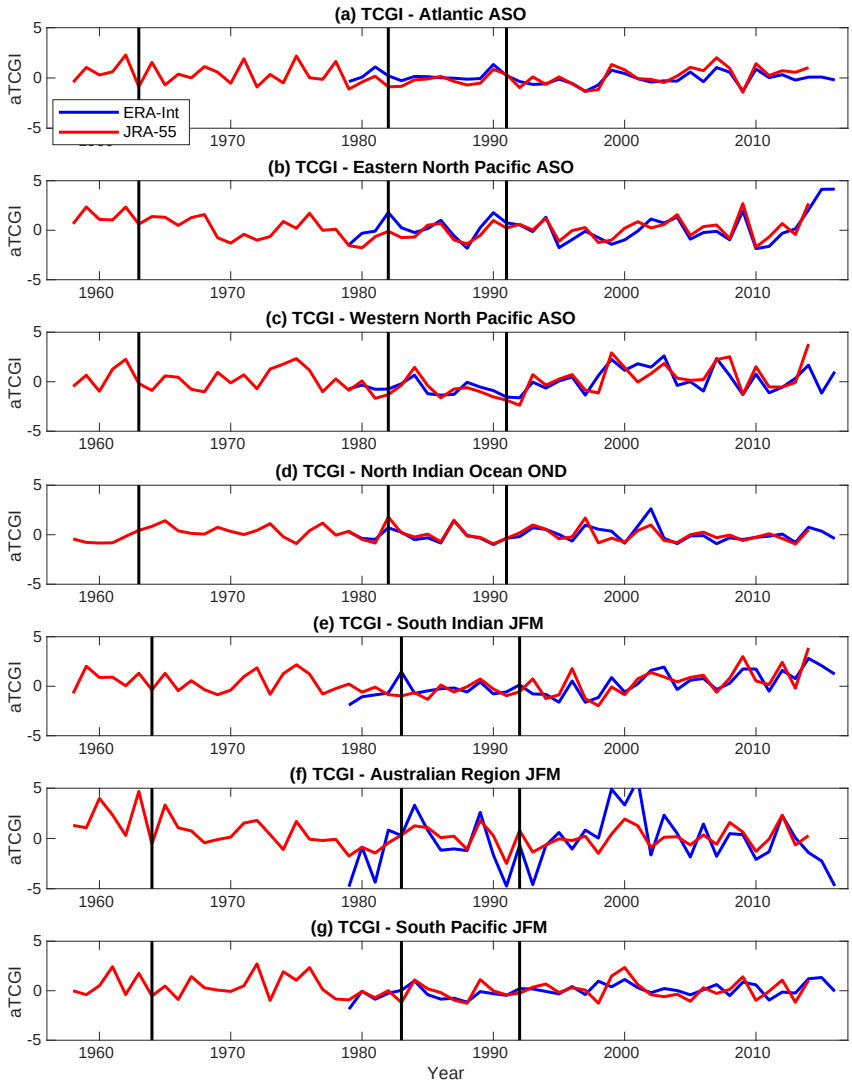

Supplementary Figure 5: Time-series of the tropical cyclone genesis (TCGI) anomalies in reanalysis: ERA-Interim (blue) and JRA-55 (red) for all basins in their peak season (August to October (ASO); October to December (OND) or January to March (JFM)). TCGI is given in counts and was multipled by 10^3. The first TC season in each hemisphere after large volcanic eruptions are marked in black.

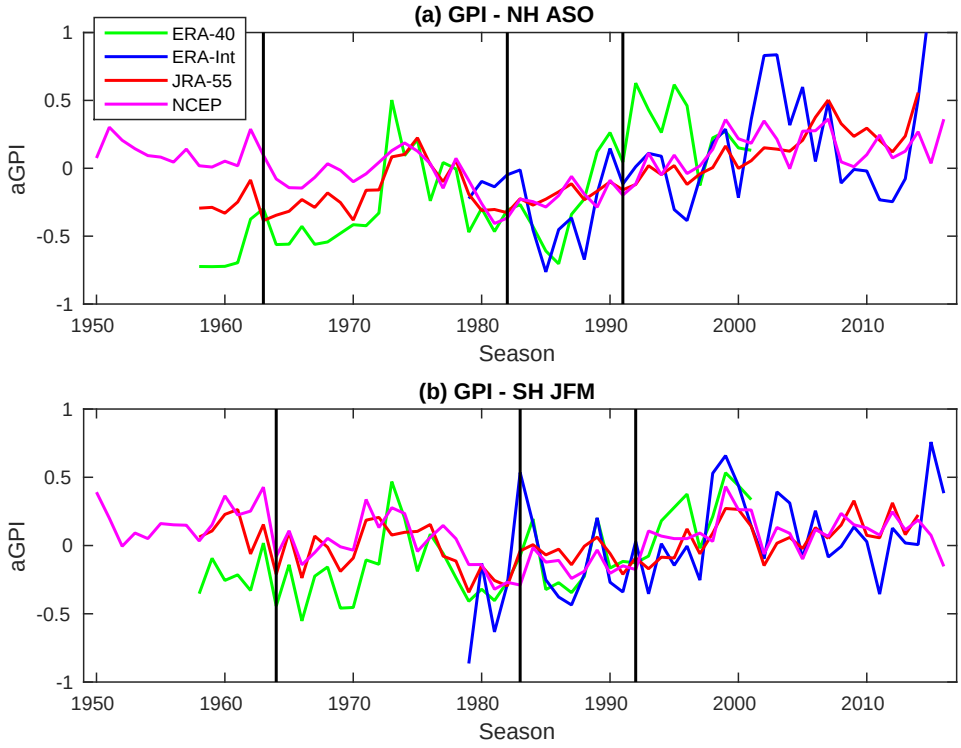

Supplementary Figure 6: Time-series of the genesis potential intensity (GPI) [1, 2] anomalies in reanalysis: ERA-40 (green), ERA-Interim (blue), JRA-55 (red) and NCEP (pink) for the (a) northern (NH) hemisphere in the August to October (ASO) (b) the southern hemisphere in January to March (JFM). GPI is dimensionless. The first TC season in each hemisphere after large volcanic eruptions are marked in black.

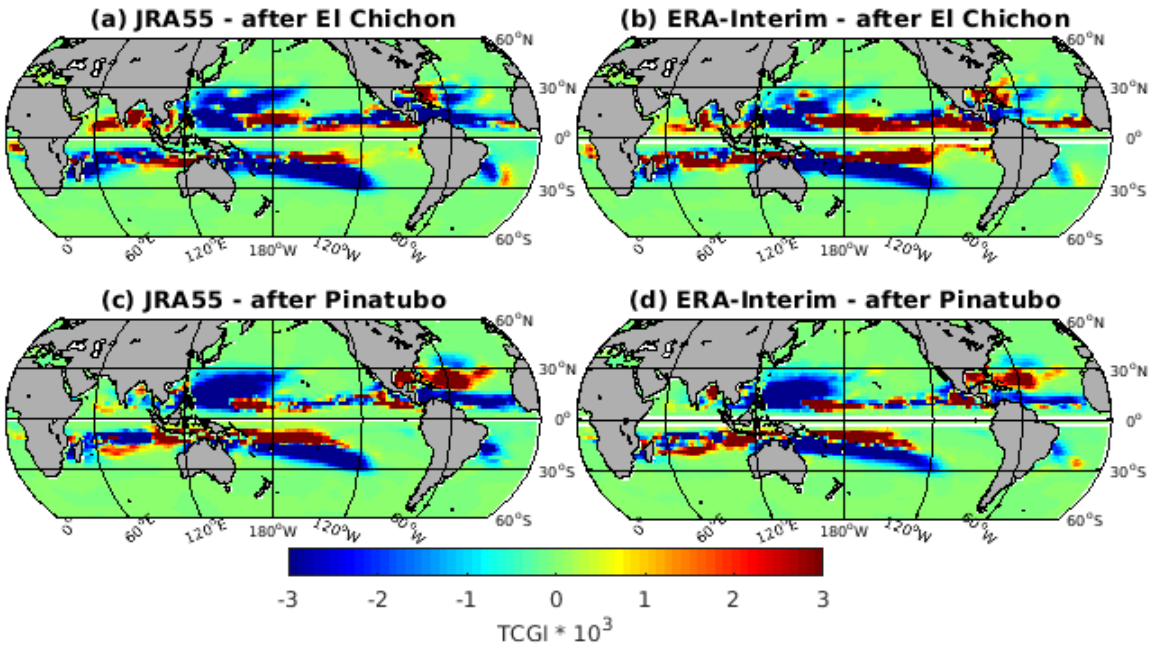

Supplementary Figure 7: TCGI anomalies in two reanalysis datasets (ERA-Interim and JRA-55) in the first TC season following the eruptions of El Chichón and Pinatubo: August to October of 1982 and 1991 in the northern hemisphere, January to March of 1983 and 1992 in the southern hemisphere, respectively.

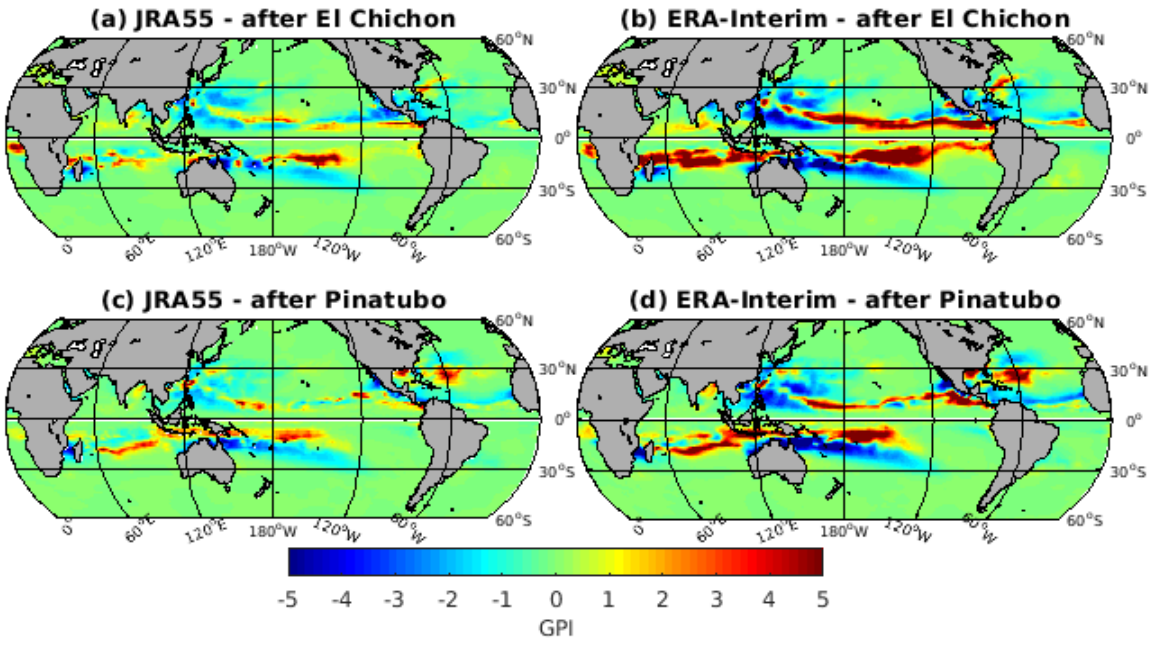

Supplementary Figure 8: GPI anomalies in two reanalysis datasets (ERA-Interim and JRA-55) in the first TC season following the eruptions of El Chichón and Pinatubo: August to October of 1982 and 1991 in the northern hemisphere, January to March of 1983 and 1992 in the southern hemisphere, respectively.

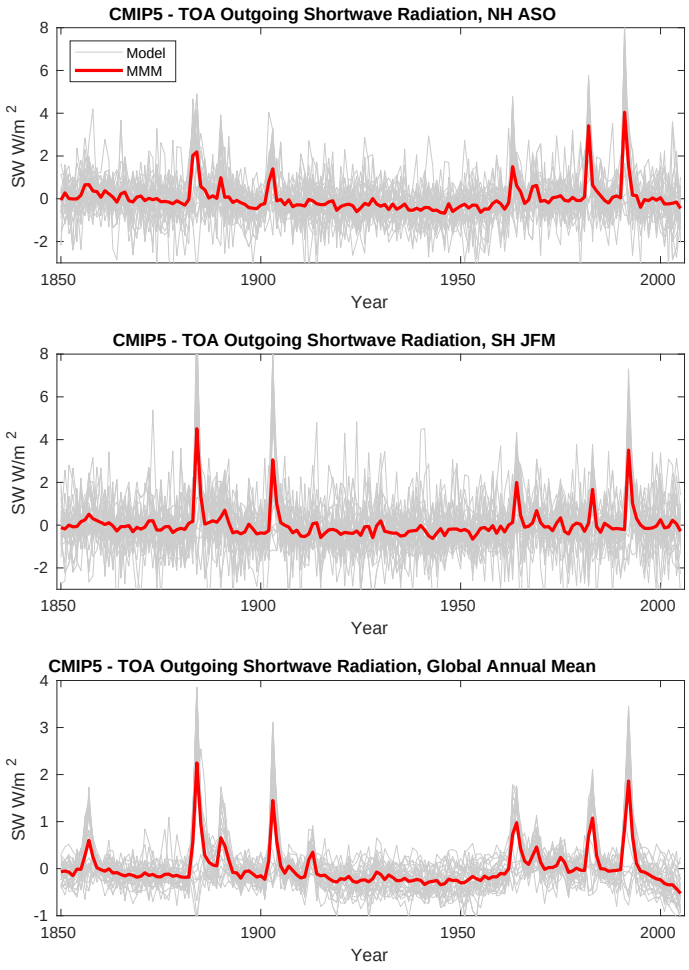

Supplementary Figure 9: Time-series of detrended anomalous outgoing shortwave radiation at the top of the atmosphere in the CMIP5 models in the (a) tropical northern hemisphere (NH) in August - October (ASO), (b) tropical southern hemisphere (SH) in January to March (JFM), (c) global annual mean. We used the 39 models for which we had data available in this plot.

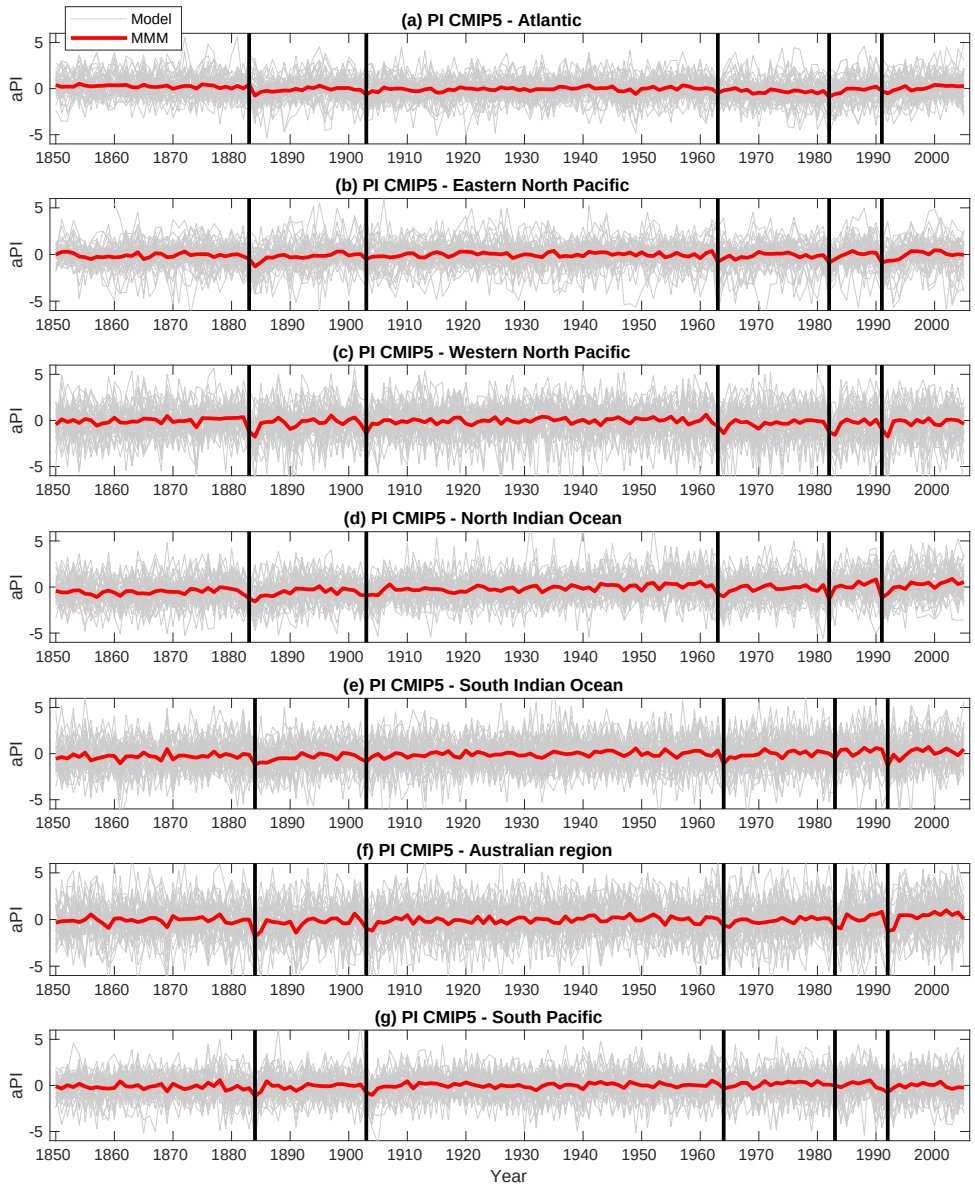

Supplementary Figure 10: Time-series of PI anomalies for individual basins in the CMIP5 models. Individual CMIP5 models are shown in the gray lines, the multi-model mean in red. The first TC season in each hemisphere after large volcanic eruptions are marked in black.

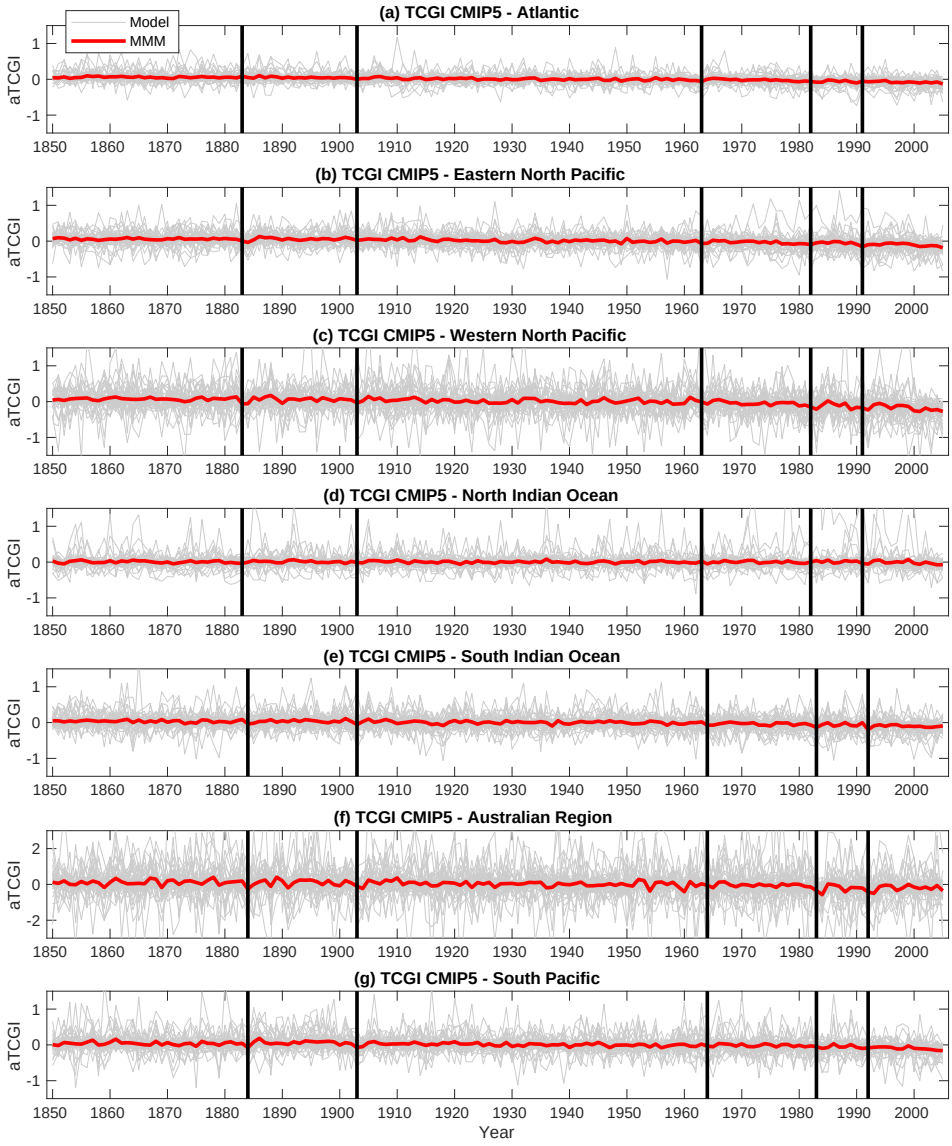

Supplementary Figure 11: Time-series of TCGI anomalies (multiplied by 10^3) for individual basins in the CMIP5 models. Individual CMIP5 models are shown in the gray lines, the multi-model mean in red. The first TC season in each hemisphere after large volcanic eruptions are marked in black.

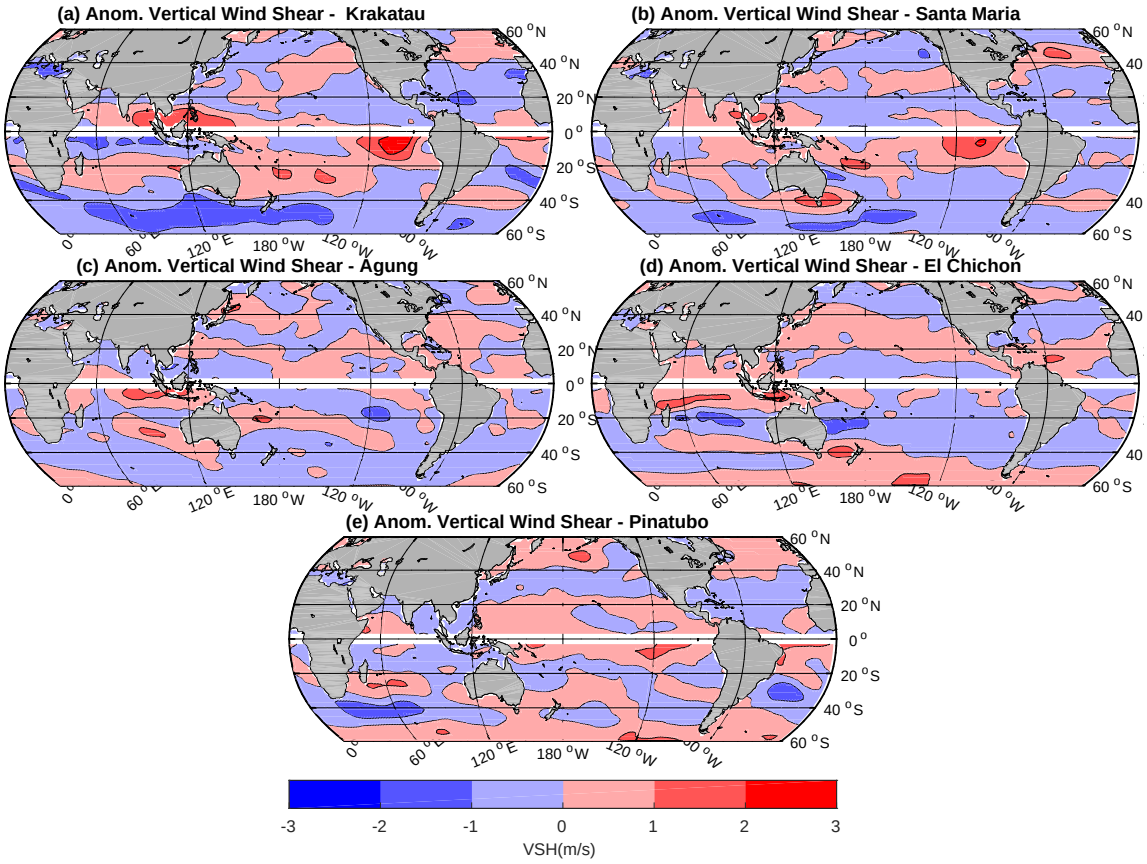

Supplementary Figure 12: Vertical wind shear (VSH) anomalies in the CMIP5 models in the first TC season following the eruptions of 5 volcanoes showing August to October in the northern hemisphere and January to March in the southern hemisphere, respectively.

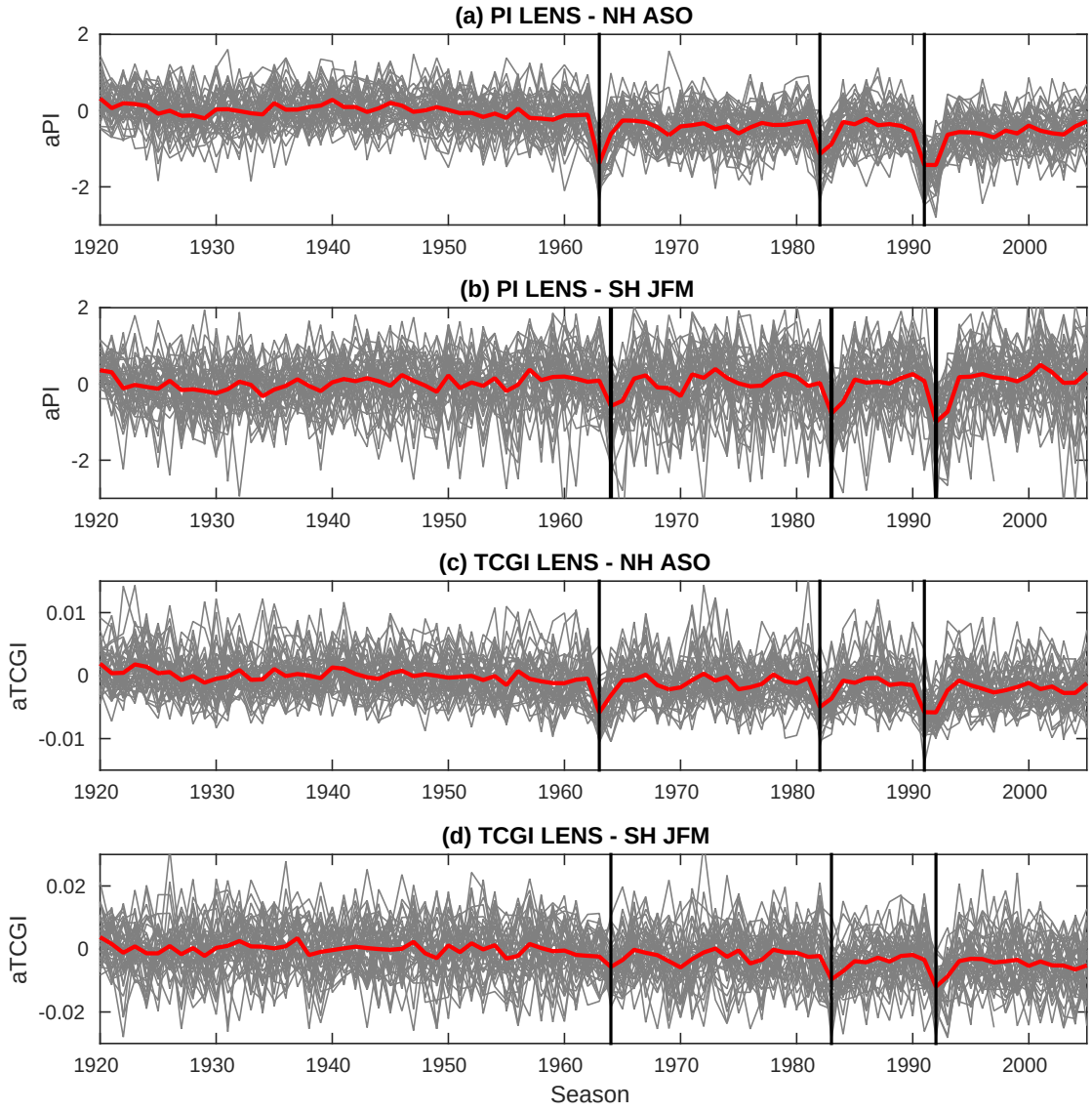

Supplementary Figure 13: Time-series of potential intensity ((a) and (b)) and TCGI ((c) and (d)) anomalies in the CESM-LENS model in the northern (NH) hemisphere in ASO and southern hemisphere (SH) in JFM. Individual ensembles are shown in the gray lines, the ensemble mean in red. The TCGI anomalies were multiplied by 10^3. PI is given in m/s, TCGI in TC counts. The first TC season in each hemisphere after large volcanic eruptions are marked in black.

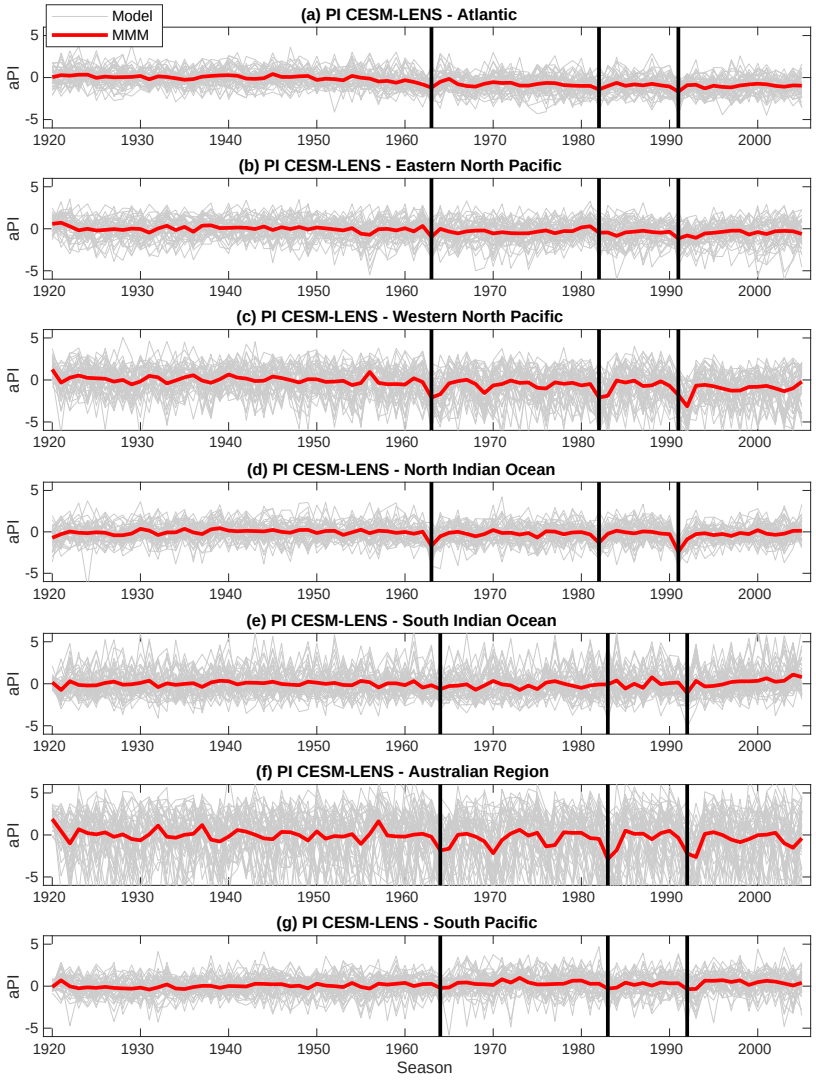

Supplementary Figure 14: Time-series of PI anomalies for individual basins in the the CESM-LENS. Individual ensemble members are shown in the gray lines, the ensemble mean in red. The first TC season in each hemisphere after large volcanic eruptions are marked in black.

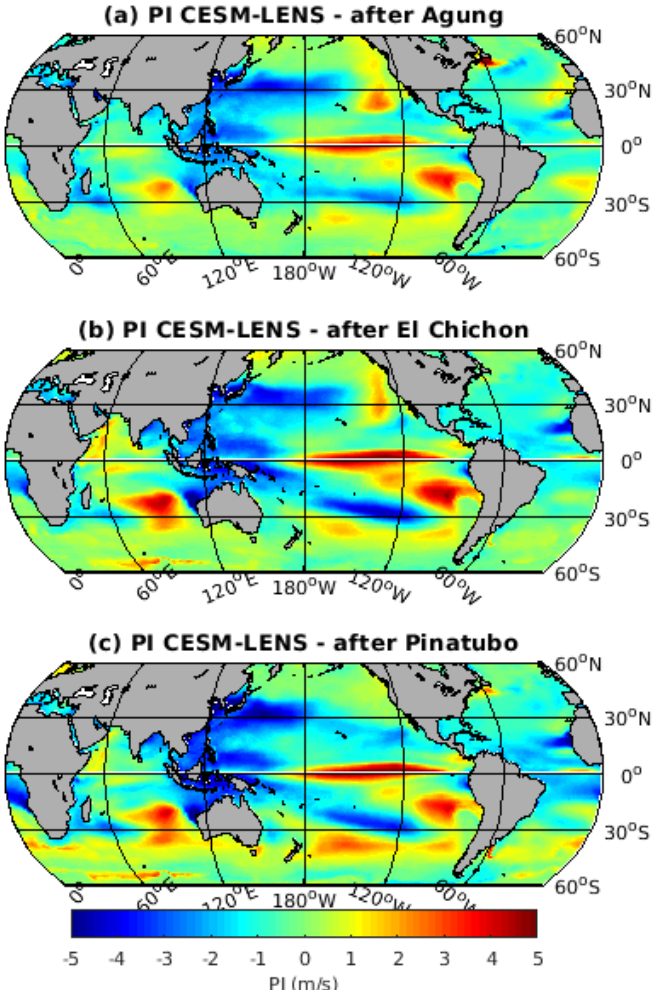

Supplementary Figure 15: Potential intensity anomalies in the first TC seasons following the eruption of Agung, El Chichón and Pinatubo: August to October in the northern hemisphere, January to March in the southern hemisphere.

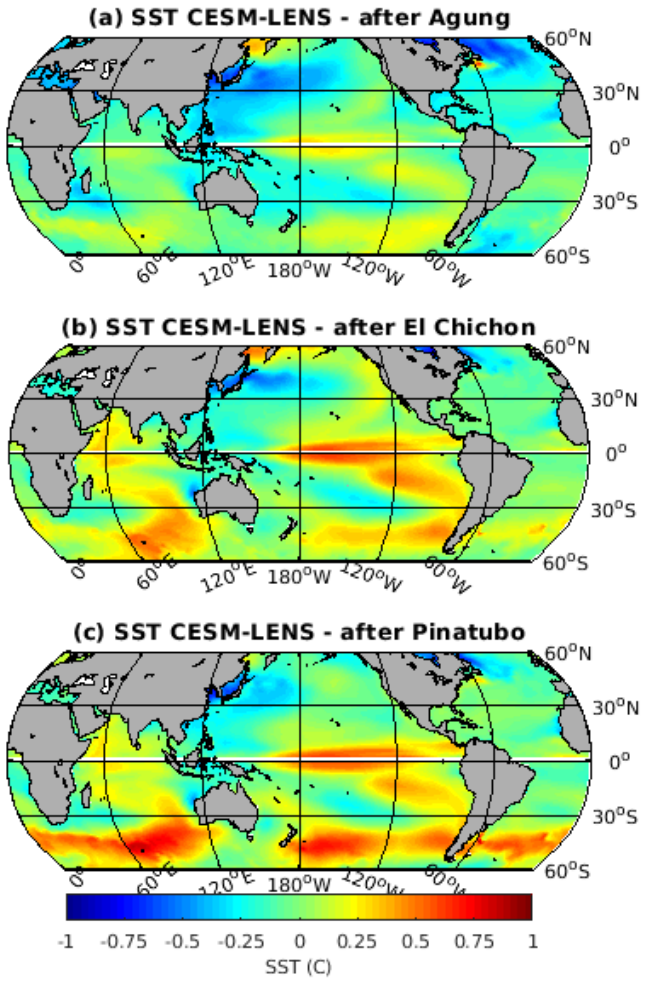

Supplementary Figure 16: Sea surface temperature anomalies in the first TC seasons following the eruption of Agung, El Chichón and Pinatubo in the first TC season following the eruption of Pinatubo: August to October in the northern hemisphere, January to March in the southern hemisphere.

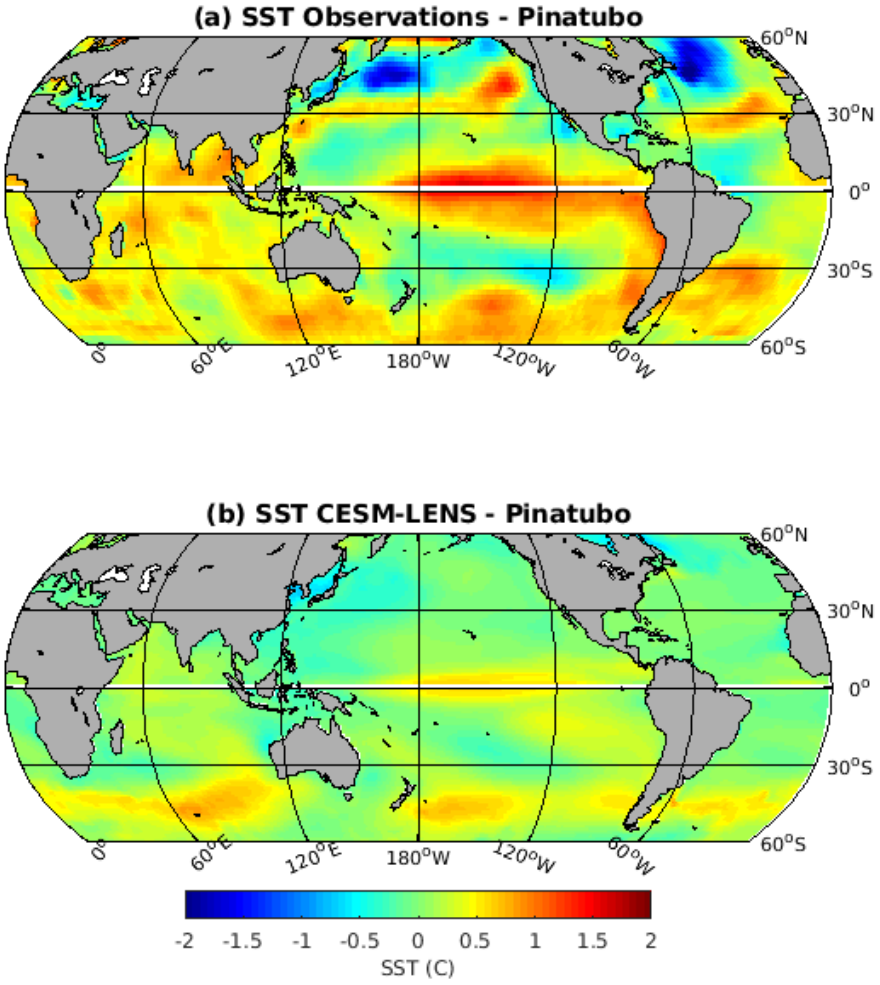

Supplementary Figure 17: Sea surface temperature anomalies in observations (a) and the multi-model CESM-LENS ensemble in the first TC seasons following the eruption of Pinatubo: August to October 1991 in the northern hemisphere, January to March 1992 in the southern hemisphere.

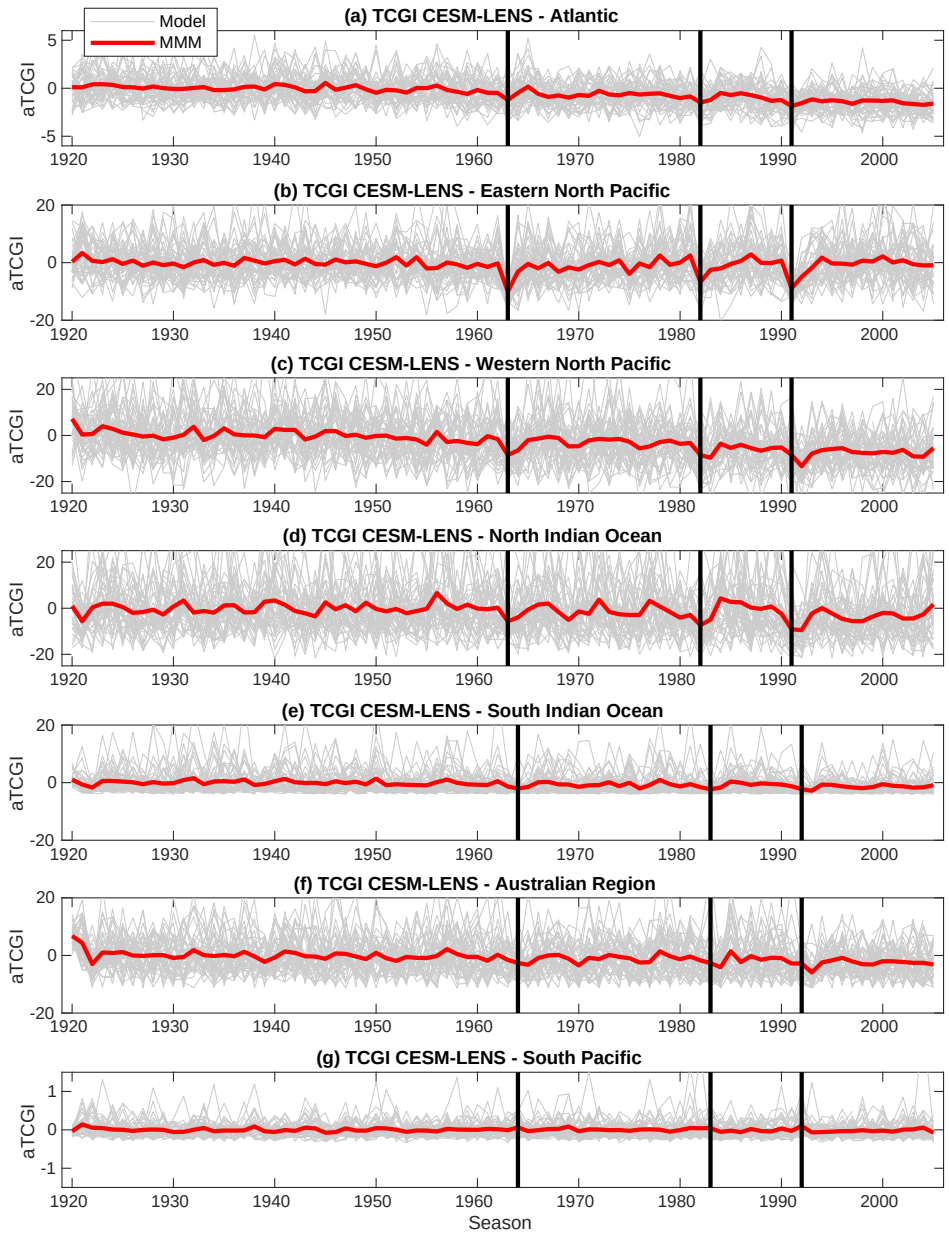

Supplementary Figure 18: Time-series of TCGI anomalies (multiplied by 10^3) for individual basins in the CESM-LENS model simulation. Individual ensembles are shown in the gray lines, the ensemble mean in red. The first TC season in each hemisphere after large volcanic eruptions are marked in black.

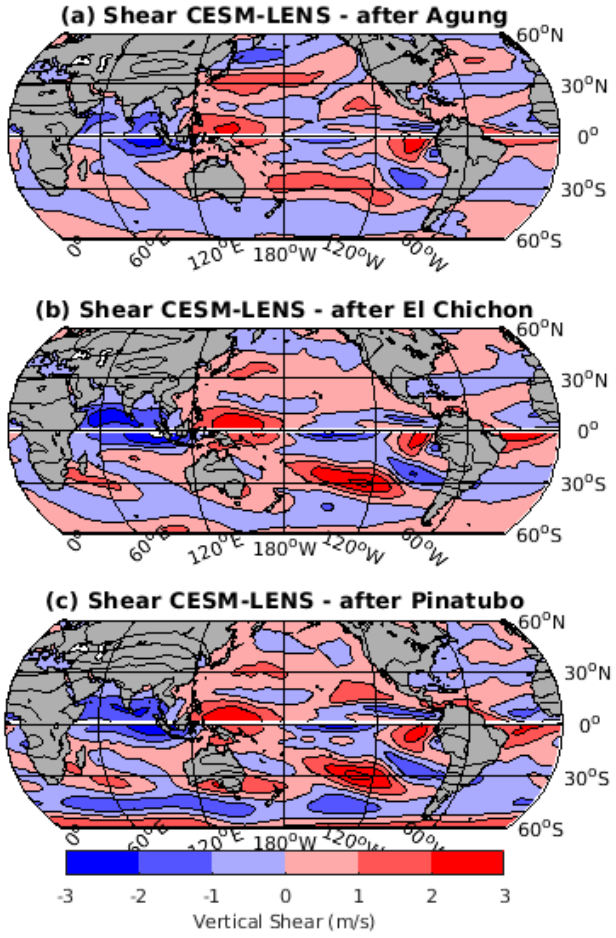

Supplementary Figure 19: Vertical wind shear magnitude anomalies anomalies in the first TC seasons following the eruption of Agung, El Chichón and Pinatubo: August to October in the northern hemisphere, January to March in the southern hemisphere.

Supplementary Table 1: CMIP5 models acronyms, number of ensembles and period for the historical simulations. Information on CMIP5 models can be found in Taylor et al. (2012) [3]. One ensemble member of each model is used in Fig. 4 of the main text. Models for which downscaled synthetic storms were generated using the Emanuel method [4, 5] in the period 1950-2005 are shown in bold. Models that we show the explicitly tracked storms as described in Camargo (2013) [6] in the period 1950-2005 are marked with an asterisk. The three models not included in the TCGI calculation are shown with a dagger †.

Model	Ens.	Period	Model	Ens.	Period
ACCESS1.0	1	1850-2005	GFDL-ESM2G	1	1861-2005
ACCESS1.3	1	1850-2005	GFDL-ESM2M	1	1861-2005
BCC-CSM1.1	3	1850-2005	GISS-E2-H	11	1850-2005
BCC-CSM1.1-m	3	1850-2005	GISS-E2-H-CC†	1	1850-2005
BNU-ESM	1	1850-2005	GISS-E2-R	16	1850-2005
CanESM2	5	1850-2005	GISS-E2-R-CC	1	1850-2005
CCSM4	6	1850-2005	HadGEM2-CC	3	1860-2005
CESM1-BGC	1	1850-2005	**HadGEM2-ES**	4	1860-2005
CESM1-CAM5	3	1850-2005	inmcm4	1	1850-2005
CESM1-CAM5.1-FV2†	4	1850-2005	IPSL-CM5A-LR	5	1850-2005
CESM1-FASTCHEM	3	1850-2005	IPSL-CM5B-LR	1	1850-2005
CESM1-WACCM	4	1850-2005	IPSL-CM5A-MR	1	1850-2005
CMCC-CESM	1	1850-2005	**MIROC5**	5	1850-2005
CMCC-CMS	1	1850-2005	MIROC-ESM	3	1850-2005
CNRM-CM5	10	1850-2005	MIROC-ESM-CHEM	1	1850-2005
CNRM-CM5.2	1	1850-2005	MPI-ESM-LR∗	3	1850-2005
CSIRO-Mk3.6.0	10	1850-2005	**MPI-ESM-MR**	3	1850-2005
FGOALS-g2	5	1850-2005	MPI-ESM-P	2	1850-2005
FGOALS-s2	3	1850-2005	**MRI-CGCM3∗**	5	1850-2005
FIO-ESM	3	1850-2005	MRI-ESM1	1	1850-2005
GFDL-CM2p1†	10	1861-2005	NorESM1-M	3	1850-2005
GFDL-CM3	5	1860-2005	NorESM1-ME	1	1850-2005

Supplementary Table 2: Rank-sum statistical test p-values results for observed TCs between the climatological distribution and seasons following volcanic eruptions in northern (NH) and southern hemisphere (SH). Variables: number of TCs(NTC), number of tropical storms (NTS), number of TCs categories 1-5 (NTC15), number of TCs categories 1-2, number of TCs categories 3-5 (NTC35), accumulated cyclone energy (ACE), lifetime maximum intensity (LMI). Locations: northern hemisphere (NH), southern hemisphere (SH). p-values below 0.05 are considered statistically significant and shown in boldface, i.e. the distributions are distinct.

Variable	Season 1		Season 2		Seasons 1+2	
	NH	SH	NH	SH	NH	SH
NTC	0.36	0.40	0.79	0.13	0.66	0.10
NTS	0.14	0.59	0.82	0.26	0.40	0.70
NTC15	0.83	0.18	0.77	0.34	0.72	0.11
NTC12	0.51	0.87	0.61	0.20	0.41	0.31
NTC35	1.00	0.90	0.06	0.81	0.19	0.95
ACE	0.36	0.18	0.79	0.28	0.66	0.09
LMI	0.05	0.26	0.32	0.08	**0.04**	0.56

Supplementary Table 3: As Table 2, but for the basins: North Atlantic (ATL), eastern North Pacific (ENP) and western North Pacific (WNP) in the period 1961-2017.

Variable	Season 1			Season 2			Seasons 1+2		
	ATL	ENP	WNP	ATL	ENP	WNP	ATL	ENP	WNP
NTC	0.10	0.80	0.92	0.16	0.45	0.33	**0.03**	0.74	0.45
NTS	0.19	0.52	0.13	0.20	0.61	0.38	0.07	0.93	0.67
NTC15	0.26	0.76	0.37	0.21	0.52	0.31	0.10	0.51	0.18
NTC12	0.32	0.53	0.74	0.06	0.49	0.32	**0.04**	0.97	0.65
NTC35	0.56	0.90	0.64	0.81	0.37	0.36	0.57	0.60	0.33
ACE	0.24	0.74	0.14	0.63	0.43	0.37	0.25	0.43	0.10
LMI	0.79	0.97	0.07	0.16	0.93	1.00	0.24	0.98	0.21

Supplementary Table 4: As Table 2, but for the basins: North Indian Ocean (NI), South Indian Ocean (SI), Australian region (AUS) and South Pacific (SP) only data in the satellite era was considered (1979-2017) and the corresponding two large volcano eruptions in that period.

Variable	Season 1				Season 2				Seasons 1+2			
	NI	SI	AUS	SP	NI	SI	AUS	SP	NI	SI	AUS	SP
NTC	0.80	0.40	0.06	**0.04**	0.75	0.43	0.36	0.75	0.98	0.98	0.53	0.23
NTS	0.97	0.78	0.23	0.32	0.28	0.44	0.30	0.82	0.48	0.76	0.93	0.38
NTC15	0.87	0.16	0.12	**0.04**	0.66	0.60	0.47	0.64	0.86	0.59	0.58	0.28
NTC12	0.77	0.28	0.24	**0.04**	0.84	0.14	0.59	0.75	0.96	0.79	0.68	0.24
NTC35	0.33	0.82	0.73	**0.04**	0.21	0.57	1.00	0.72	0.87	0.57	0.81	0.26
ACE	0.32	0.51	0.97	**0.03**	0.83	0.78	0.18	0.55	0.60	0.81	0.33	0.29
LMI	0.30	0.25	0.26	0.28	0.33	0.44	0.60	0.62	0.98	0.18	0.70	0.70

Supplementary Table 5: As Table 2, but for TC-like storms in the CMIP5 models.

Variable	Model	Season 1		Season 2		Seasons 1+2	
		NH	SH	NH	SH	NH	SH
NTC	MPI	0.29	0.59	**0.01**	0.78	**0.01**	0.86
	MRI	0.29	0.86	**0.03**	0.70	0.45	0.70
ACE	MPI	0.76	0.95	**0.03**	0.88	0.09	0.95
	MRI	0.31	0.91	0.13	0.82	0.73	0.82
LMI	MPI	**0.01**	0.92	0.28	0.60	0.22	0.78
	MRI	0.22	0.66	0.43	0.29	0.76	0.67

Supplementary Table 6: As Table 2, but for synthetic TCs. Models 1-6 are given in Table 1 in boldface.

Variable	Model	Season 1		Season 2		Seasons 1+2	
		NH	SH	NH	SH	NH	SH
NTC	1	0.38	0.17	0.71	0.90	0.82	0.48
	2	0.17	0.26	0.17	0.17	0.06	0.09
	3	0.17	0.71	0.90	1.00	0.31	0.82
	4	1.00	0.17	0.90	0.17	0.94	0.06
	5	1.00	0.90	0.55	0.71	0.70	0.70
	6	0.09	0.26	0.17	**0.05**	**0.04**	**0.04**
NTC15	1	0.26	0.26	1.00	1.00	0.48	0.48
	2	0.26	0.26	0.71	0.38	0.31	0.18
	3	0.17	1.00	0.90	1.00	0.31	1.00
	4	0.90	0.17	0.71	0.38	0.70	0.13
	5	0.90	0.26	0.38	0.26	0.70	0.13
	6	0.09	0.26	0.09	0.38	**0.03**	0.18
NTC35	1	0.38	0.09	0.90	0.09	0.70	0.59
	2	0.55	0.55	0.90	0.55	0.59	0.70
	3	0.26	0.55	0.55	0.55	0.24	0.24
	4	1.00	0.90	0.38	0.90	0.59	0.70
	5	0.55	0.09	**0.02**	0.09	0.06	**0.02**
	6	**0.02**	0.38	0.17	0.38	**0.02**	0.39
ACE	1	0.38	0.09	0.90	0.71	0.70	0.48
	2	0.55	0.55	0.71	0.71	0.48	0.48
	3	0.38	0.55	0.90	0.26	0.48	0.24
	4	0.71	0.26	0.71	0.17	0.48	0.09
	5	1.00	0.09	0.17	0.09	1.00	**0.03**
	6	**0.05**	0.26	0.09	0.55	**0.01**	0.24
LMI	1	0.21	0.73	0.94	0.56	0.36	0.52
	2	0.20	0.66	0.47	0.35	0.16	0.74
	3	0.65	0.56	0.68	0.68	0.54	0.49
	4	0.58	0.90	0.20	0.82	0.62	0.80
	5	0.92	0.39	**0.01**	0.21	0.07	0.80
	6	0.53	0.39	0.94	0.96	0.71	0.58

Supplementary References

[1] Emanuel, K. A. & Nolan, D. S. Tropical cyclone activity and global climate. *Bull. Amer. Meteor. Soc.* **85**, 666–667 (2004).

[2] Camargo, S. J., Emanuel, K. A. & Sobel, A. H. Use of a genesis potential index to diagnose ENSO effects on tropical cyclone genesis. *J. Climate* **20**, 4819–4834 (2007).

[3] Taylor, K. E., Stouffer, R. J. & Meehl, G. A. An overview of CMIP5 and the experiment design. *Bull. Amer. Meteor. Soc.* **93**, 485–498 (2012).

[4] Emanuel, K., Ravela, S., Vivant, E. & Risi, C. A statistical deterministic approach to hurricane risk assessment. *Bull. Amer. Meteor. Soc.* **87**, 299–314 (2006).

[5] Emanuel, K. A. Downscaling CMIP5 climate models shows increased tropical cyclone activity over the 21st century. *Proc. Nat. Acad. Sci.* **110**, 12219–12224 (2013).

[6] Camargo, S. J. Global and regional aspects of tropical cyclone activity in the CMIP5 models. *J. Climate* **26**, 9880–9902 (2013).